PHYSICAL REVIEW B VOLUME 55, NUMBER 20 15 MAY 1997-II

Effect of metal band characteristics on resonant electron capture: H^- formation in the scattering of hydrogen ions on Mg, Al, and Ag surfaces

M. Maazouz, A. G. Borisov, V. A. Esaulov, J. P. Gauyacq, L. Guillemot, S. Lacombe, and D. Teillet-Billy
Laboratoire des Collisions Atomiques et Moléculaires, Unité associée au CNRS, Université Paris–Sud, bât 351, 91405 Orsay, France

(Received 14 February 1996; revised manuscript received 5 November 1996)

We present the results of an experimental and theoretical study of H^- formation in collisions of 1 to 4 keV positive and negative hydrogen ions with clean Mg, Al, and Ag surfaces. Ion fractions and energy loss spectra of scattered particles were measured in a large angular range allowing us to investigate the characteristics of the resonant charge transfer process for a wide range of collision velocities normal to the surface, thus probing the charge-transfer process in different atom-surface distance ranges. We compare H^- formation on metal surfaces, with different valence-band characteristics involving the work function and Fermi energies (ϵ_F). The experimental results are found to be in good agreement with the predictions of the nonperturbative coupled angular mode method, used in conjunction with a semiclassical rate-equation approach. The importance of the parallel velocity effect is demonstrated and the differences between the various metal targets are interpreted in terms of differences between both work functions and also the valence-band width or Fermi energies. [S0163-1829(97)01220-4]

I. INTRODUCTION

This paper presents the results of a joint experimental and theoretical study of electron-capture processes in hydrogen ion scattering on Mg and Ag surfaces. The objective of this work is a study of H^- formation on clean, high work-function (ϕ) metal surfaces, with different valence-band characteristics (ϕ and Fermi energies ϵ_F). It extends our recent study of scattering on Al.[1] On metal surfaces H^- formation involves a transition of an electron from occupied levels of the valence band to the H^- level, the latter being downward shifted due to image potential effects as is schematically illustrated in Fig. 1. For many common clean metals, the large value of the work function ϕ requires a large shift and so H^- formation can only occur at very small atom-surface distances. Electron capture in these cases is favored by the rapid movement of the atom parallel to the surface, due to a kinematic matching of energies of electrons in the solid[2–5] and in H^- when viewed from the reference frame of the moving H.

Previously,[1] we reported experimental and theoretical results for H^- formation in 1- to 4-keV H^+ collisions on Al surfaces over a large domain of scattering conditions, for which the final charge state distribution is determined at very different atom-surface separations. We showed that the nonperturbative coupled angular mode (CAM) method,[6] in conjunction with a semiclassical rate equation approach[3,4] gave a good description of this dynamical charge-transfer process over a large range of scattering conditions. It extended previous works on Al(111),[7] corresponding to very grazing scattering conditions and thus probing very large atom-surface distances

In previous works, detailed studies on H^- formation have been reported[4] in the case of metal targets partly covered with alkali atoms, which allowed a discussion of the effect of the surface work function. The effects of varying the metal valence-band width were not discussed. In this paper we compare H^- formation on clean, high work-function (ϕ) metal surfaces, with different valence-band characteristics. Indeed, regarding ‘‘jellium’’ characteristics, Al and Ag have practically the same work functions $\phi = 4.4$ eV (Al) and $\phi = 4.3$ eV (Ag) while Fermi energies differ by a factor of 2 ($\epsilon_F = 11.65$ eV for Al compared to $\epsilon_F = 5.49$ eV for Ag). The energy of the bottom of the conduction band is $U_0 = 15.9$ eV (Al). and $U_0 = 9.79$ eV (Ag). Mg has the smallest work function $\phi = 3.64$ eV and its Fermi energy and the bottom of the conduction band are close to those of Ag ($\epsilon_F = 7.08$ eV and $U_0 = 10.72$ eV). We will show that in contrast to intuitive ideas H^- formation is governed in the present case not only by the values of the work function but also by the so-called angular distribution of the transfer probability which is an internal property of the charge transfer related to the energy position of the bottom of the metal conduction band. This is related to the fact that H^- formation in the studied systems is due to the so-called parallel velocity effect, the energy difference between the ionic level and the Fermi level being bridged by the collision velocity.

II. EXPERIMENT

A detailed description of the apparatus used for the present experiments is given elsewhere.[8] Briefly H^+ and H^- ions are produced in a discharge source, mass selected, and deflected through 90° to eliminate photons and neutrals before entering into the main UHV chamber. The pressure in the chamber is of typically 5×10^{-10} torr. The apparatus is equipped for measurement of electron and ion energy spectra using tandem parallel-plate energy analyzers, as well as time-of-flight (TOF) scattering and direct recoil spectroscopy.

Polycrystalline Mg and Ag samples were used. The metals in question are what is usually regarded as ‘‘free-electron

0163-1829/97/55(20)/13869(9)/$10.00

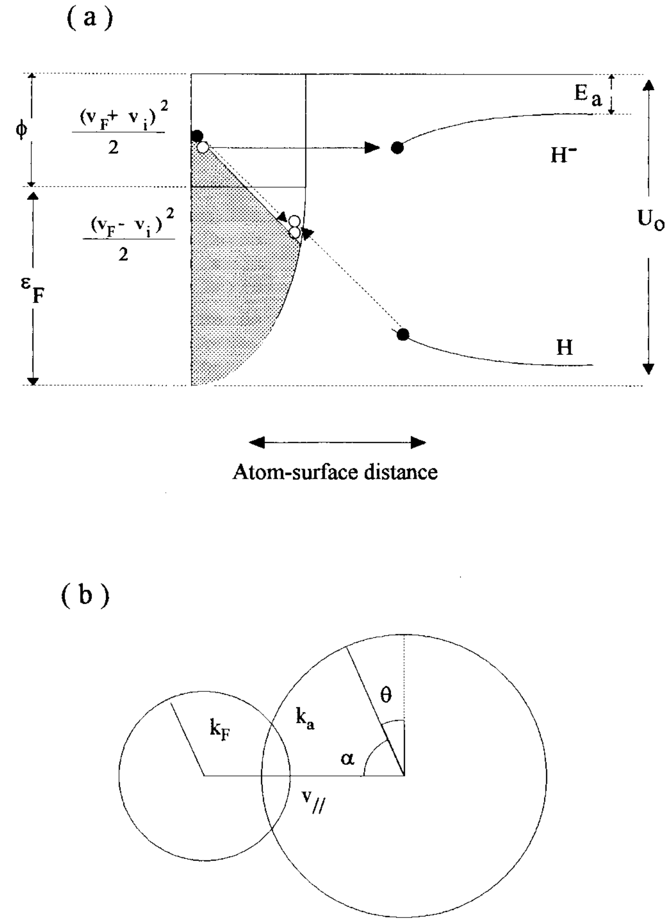

FIG. 1. (a) Schematic diagram of the energy levels of the metal-hydrogen atom/ion system, relevant to the resonant electron-capture process and the Auger ionization mechanism discussed in Sec. V. The hatched area represents the kinematically modified distribution of occupied target electronic states. The resonant electron capture (solid line) and kinematic Auger ionization (dashed lines) are schematized by the arrows. (b) Schematic diagram of the shifted Fermi sphere model. The k_a sphere represents, in k space, the electronic states, which are degenerate with the atomic state and the k_F sphere represents the Fermi sphere. The Fermi sphere is shifted by an amount given by the component of the collision velocity parallel to the surface.

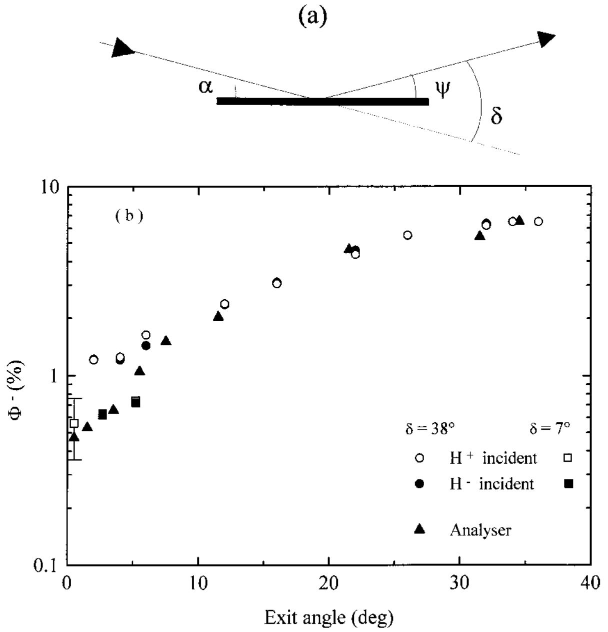

FIG. 2. (a) Definition of the angle naming convention for scattering. (b) H^- charge fractions as a function of the exit angle with respect to the surface for Ag.

metals'' and a jelliumlike description is usually considered suitable in most theoretical works on charge transfer as well as in this one. Therefore the fact that the samples are polycrystalline does not seem important. The samples were hand polished to 0.05 μm and had a mirrorlike appearance. *In situ* preparation consisted of repeated cycles of small angle (less than 10°) Ne^+ sputtering and annealing. Because, as we shall see below, surface flatness is an important consideration in these measurements, in the final stage of preparation the samples were subjected to prolonged more grazing incidence (circa 4°) Ne or Ar bombardment. A direct measurement of the degree of surface flatness could not be performed in our setup, using, e.g., a scanning tunneling microscope. Measurements of the angular distributions of scattered H atoms incident at a 3.5° angle on the surface were performed. This distribution had a full width at half maximum (FWHM) of 6° with a tail extending to large angles. This distribution is wider than reported in previous grazing incidence studies[7] though a direct comparison is not possible since those authors report results for a much more grazing incidence angle of 0.8°, for which they report a FWHM of 0.8°. However, the residual roughness plays a positive role allowing us to perform measurements over a wide scattering angular range. As we shall see below, a correction for the residual roughness for grazing scattering could be made using our time-of-flight measurements. The conclusions of this paper however will not rely on the data for the lowest angles.

The surface cleanliness was ascertained by measuring TOF spectra of scattered and recoiled particles under Ar bombardment. The surface was assumed to be cleaned when statistically significant peaks of recoiled O and H were no longer observed.

H^--ion fraction (ϕ^-) measurements were made for ion energies in the 1–4-keV range. Several approaches were used. In the first mode measurements were made for fixed scattering angles [δ, see Fig. 2(a)] of 8° and 38° using position sensitive 30-mm diameter channelplate detectors set at a distance of 2.2 m from the scattering center at the end of time-of-flight analysis tubes. These detectors are equipped with three discrete anodes. A deflector plate assembly set before the channelplates allows us to separate the incoming positive and negative ions and neutrals, which can thus be detected simultaneously by each of the anodes. The sample orientation was varied and incidence angles (α) changed in the 2° to 36° range (as measured with respect to the *surface plane*), allowing us to sample a similar exit angle (ψ) range. Initially charge fractions were determined by counting scattered ions and neutrals using a continuous beam. Time-of-flight spectra for each charge state were then recorded for various angular settings and the charge fractions were determined from these spectra. In all these measurements we assumed an *equal detector efficiency for ions and neutrals.*

This assumption seems reasonable on the basis of our earlier studies of negative-ion scattering[9] for energies above 1 keV. Note that care was also taken to eliminate the effect of the Earth's magnetic field by installing compensating Helmholtz coils along the time-of-flight tubes.

The second method consisted of determining the angular distributions of scattered particles and the associated charge fraction for a fixed incident angle α, but for a range of scattering angles with respect to the incident-beam direction, using one of the rotatable parallel-plate spectrometers. A channel electron multiplier set behind the analyzer was used to count successively neutrals+ions and neutrals. Ions were counted separately on the channel plate detector set at the exit slit of the analyzer. The exit slit width was of 40 mm, allowing a simultaneous collection of ions within energies ranging from, e.g., the incident energy E_0 to $0.8E_0$. Using two different detectors, a relative value of the ion fraction was thus obtained. The ion fraction was then normalized to the one obtained with the 38° TOF tube detector. The characteristics of results by these methods are discussed in the next section.

III. RESULTS

A. Scattering on Ag

Typical results of ion fraction measurements for the Ag surface are shown in Fig. 2(b) for a 4-keV incident ion energy as a function of the exit angle to the surface ψ, using the different approaches mentioned above. The overall trend of these results is that the negative-ion fraction is found to increase as a function of ψ and attains a value of about 6% for large angles. In order to verify the *influence of the incoming ion trajectory* on Φ^- we performed measurements with both H^- and H^+ beams. The results using the incident negative-ion beam are compared with those using the H^+ beam in Fig. 2(b). As may be seen, *similar results are obtained, indicating that the memory of the incident ion charge state is lost.*

We shall now briefly discuss some differences observed in our results for small exit angles. Measurements were made using the rotatable analyzer for an incidence angle of 3.5° with respect to the surface plane. For this incidence angle one has a condition of specular scattering for the 7° TOF tube detector. For this α one should obtain the same result when using the analyzer and the 7° and 38° TOF tube detectors. We find indeed that the data obtained using the movable analyzer (corresponding to small incidence angles) follow the trend of the 7° detector for small ψ and that of the 38° detector for larger ψ. Note that the analyzer data were normalized to the 7° TOF tube detector data.

A peculiar feature of these results however, is that for small exit angles there is a difference in the value of Φ^- obtained using the 38° TOF tube. The 7° TOF tube data lie lower than the 38° one. In the initial stages of these measurements, the low ψ, 38° data corresponded to still larger values of Φ^-. Smaller fractions were obtained after prolonged grazing incidence sputtering, leading us to believe that these larger values correspond to a greater sensitivity of the H^- yield to residual surface imperfections, for conditions in which the incidence angle is large and the exit angles are small. Indeed in case of the 38° detector small ψ correspond to very large incidence angles, when many of the scattered particles penetrate into the solid and hence the scattering into the small exit angles should be more strongly affected by residual surface-roughness effects than for specular scattering conditions, when the particles stay further away from the surface. We interpret the aforementioned agreement between the results obtained using the analyzer and the small (7°) and large (38°) TOF tube data, as confirming the above conclusions concerning surface roughness. The fact that the H^- fraction increases with increasing surface roughness is known and has been commented upon in earlier studies.[7] We conclude that the correct general shape of the ion fraction corresponds to the trend given by the analyzer data, the 7° TOF tube for small ψ and the 38° TOF tube for medium and large ψ. Only the 7° TOF tube for small ψ and the 38° TOF tube for medium (above 6°) and large ψ data will be presented in the following.

Figure 3(a) shows some measured TOF spectra for scattered neutrals obtained for 4-keV incident ions and for scattering with $\alpha = 3.5°$ for $\psi = 3.5°$ and 34.5° and also $\alpha = 19°$ for $\psi = 19°$. For small incidence, specular, scattering a fairly narrow spectrum is obtained corresponding to an average energy loss of 200 eV and a peak FWHM of the order of 200 eV, while for the larger exit angle a high-energy-loss tail extending to losses of up to 1.6 keV is observed. In case of the 19° incidence the spectrum is broader, having a larger component of medium-energy losses. The energy losses we observe for Ag are smaller in magnitude than those we observed for H scattering on Al.[1] We shall not dwell on a discussion of energy losses here (see Ref. 10). The spectra of scattered ions had similar general shapes.

The ion fractions reported above corresponded to a sum over the full energy-loss range. H^- fractions corresponding to low-energy losses ($\delta E \leqslant 400\,\text{eV}$) were determined from these spectra. No significant difference from the summed ion fraction was observed. This is due to the fact that as a function of energy, the difference in ion fractions at large angles is not very large. Therefore, even though energy losses of up to 1600 eV are observed under certain conditions, the integrated ion fraction is not very different than the one corresponding to small losses. Note that this also accounts for the fact that the analyzer data (Fig. 2), which corresponded to a 20% fraction of energy losses (given the analyzer exit slit width) lies close to the 38° TOF tube data.

A very interesting *difference is however observed for the grazing incidence* scattering spectra. Figure 3(b) shows the TOF spectrum for scattered neutrals and negative ions for $\phi = 3.5°$ and specular reflection for a 4-keV energy. We observe what appears like a larger energy-loss shift of the H^- spectrum and a broader peak. Also plotted in the figure is the negative-ion fraction calculated as the ratio of the peak areas of ions over neutrals obtained by progressively integrating the peak areas for increasingly large-energy losses. We observe that the charge fraction is lower for the lower-energy-loss particles. The higher-energy losses correspond to particles that penetrate deeper into the solid and, as for the case of the 38° data discussed above, these should be more sensitive to local imperfections leading on an average to larger fractions than the more ‘‘ideal specular reflection.’’ Such differences were not observed for the larger-angle scattering spectra in Fig. 3(a).

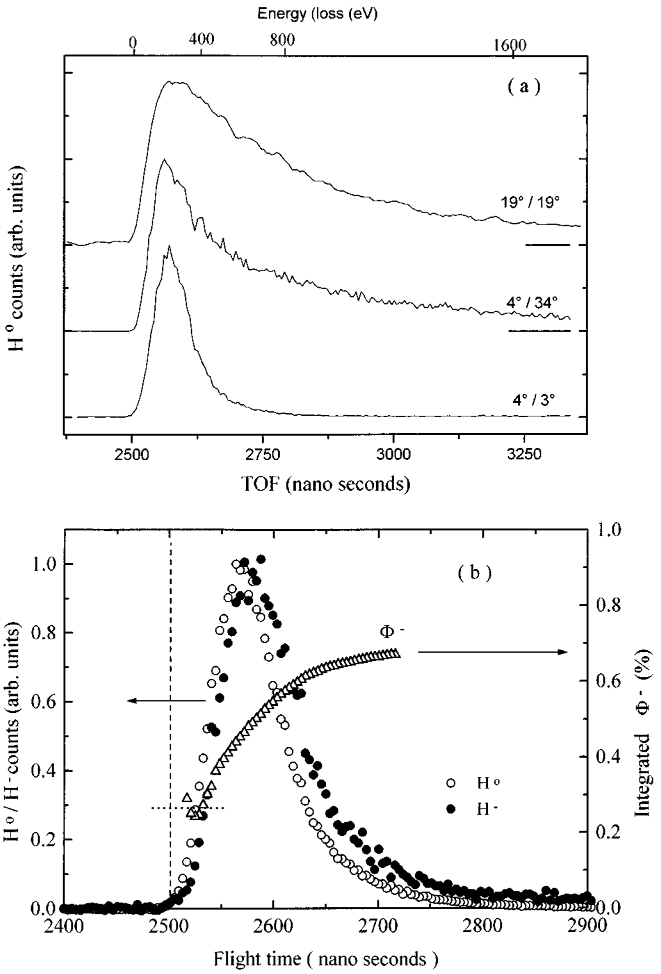

FIG. 3. (a) Time-of-flight spectra of scattered hydrogen atoms for the indicated incidence (left) and exit (right) angles. (b) Time-of-flight spectra of scattered hydrogen atoms and negative ions for a 3.5° incidence and exit angles. Also shown is the ion fraction that is deduced from the ratios of the peak areas integrated over increasing energy-loss regions. The vertical bar indicates the incident (unscattered) ion flight time. The horizontal line indicates the average value of Φ^- used in Fig. 4.

The incidence energy dependence of the H^- fraction is illustrated in Fig. 4 by comparing the data for 1 and 4 keV. The *ion fraction increases considerably with increasing ion energy*. This figure also gives Φ^- for the limiting value for low-energy losses for the 3.5° specular reflection [the 4-keV ''corrected'' data point, taken from Fig. 3(b)] and suggests a more rapid decrease of the ion fraction as ψ decreases.

The positive-ion fractions Φ^+ we determined were smaller than Φ^-. Thus for a 4-keV incident energy and $\alpha = 4°$, Φ^+ represented about 1% for $\psi = 4°$ and 2% for $\psi = 34°$. Similar positive-ion fractions were found for both H^- and H^+ incident ions.

B. Scattering on Mg

Figure 5 summarizes our results of H^- production on Mg. The negative-ion fraction increases as a function of ψ and attains a value of about 10% for large angles for a 4-keV energy. The positive-ion fractions are smaller. Φ^+ increased from about 0.7% to 1.3% at 1 keV and from 1.2% to 2% at

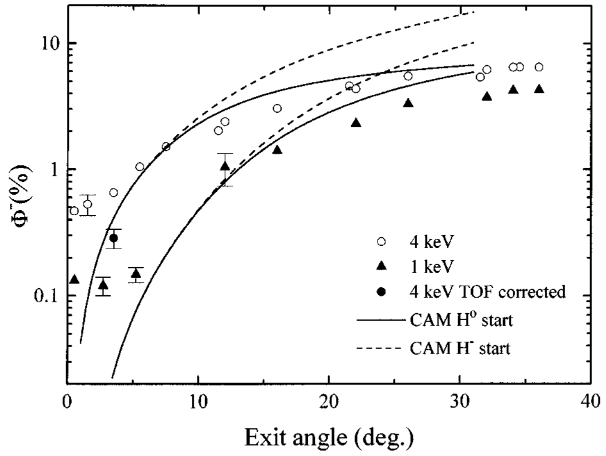

FIG. 4. Experimental and theoretical H^- fractions for a 1- and 4-keV ions incident on Ag. The corrected value was taken from Fig. 3(b).

4 keV in the studied ψ range. As for Ag the ion fractions were independent on the incident ion charge state: H^+ or H^-.

TOF spectra for a 4-keV incident energy are shown in Fig. 6. In this case, contrarily to the Ag case reported above, we observe rather large-energy losses. Integration of peak areas for the small-energy-loss region yielded ion fractions, which were not significantly different from the summed ones, corresponding to the continuous beam measurements. This may appear surprising given the large losses, since on the basis of the data for silver one might expect a larger fraction at higher energies. The reason for this becomes clear when one examines the energy and angular dependence of the ion fractions for Mg. An interesting feature of the angular dependence of the ion fraction as a function of energy (Fig. 5) is that, while at small ψ a substantial difference between the results for 1 and 4 keV is observed, they are of the same order of magnitude at large angles. This explains that the large-energy losses do not affect the value of the ion fraction at big exit angles. A previous study of D^- formation on an Mg surface was performed earlier by Shi, Rabalais, and Esaulov[11] who reported ion fractions for a 6° incidence and

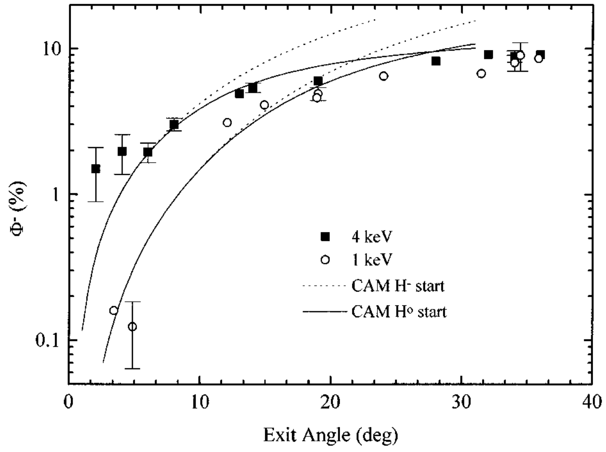

FIG. 5. Experimental and theoretical H^- fractions for a 1- and 4-keV ions incident on Mg.

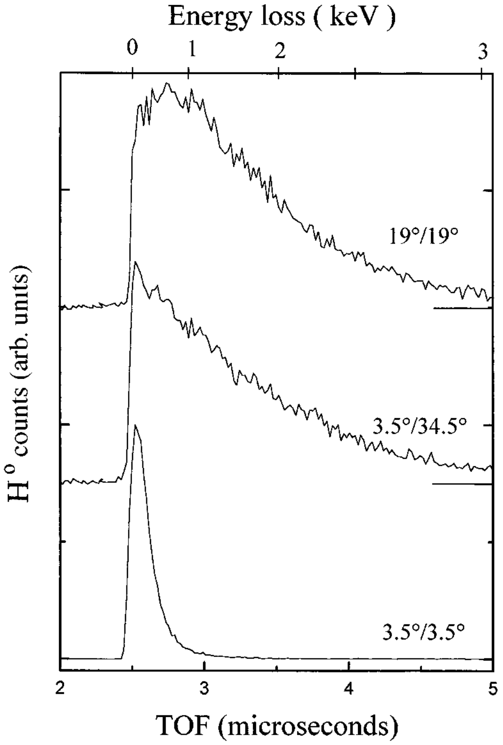

FIG. 6. Time-of-flight spectra of hydrogen atoms scattered from Mg, for the indicated incidence (left) and exit (right) angles.

16° exit angle with respect to the surface plane in an energy range from 1.5 to 4 keV. Their results may be compared with the present one after scaling to the same velocities. Reasonably good agreement is found for high energies. Thus at 3 keV (approximately equivalent to 2 keV for H) they found a D^- fraction of 5% in good agreement with our results at this energy shown in Fig. 7. At lower energies their results lie lower. We attribute this to the lack of compensation of the Earth's magnetic field in those measurements.

C. Comparison of results for Mg, Al, and Ag surfaces

Let us now compare the results for the various surfaces studied. Figure 7 shows the measured Φ^- for a 2-keV incident energy for the Mg, Al, and Ag targets. As may be seen the trend of the data as a function of the exit angle is similar in all cases. The H^- fractions turn out to have similar magnitudes for the Al and Ag surfaces. The ion fraction for Mg is considerably higher.

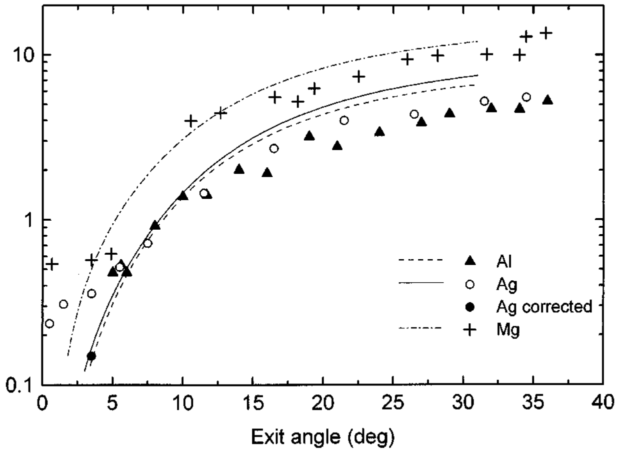

FIG. 7. Experimental (a) and theoretical (b) H^- fractions for 2-keV H^+ incident on Mg, Al, and Ag. Theoretical results are obtained for H initial conditions (see text).

IV. DISCUSSION

A. Calculations of the H^- fractions

The H^- fractions are obtained in the same way as in our previous study.[1,12] Briefly, the evolution of the H^- population, due to the charge transfer between the ion and a jellium metal surface P^- is described within a rate equation approach, well justified for the case of large surface temperatures or high parallel velocities $(v_\parallel)$.[13–16]

$$\frac{dP^-}{dt} = -\Gamma^l P^- + \tfrac{1}{2}\Gamma^c(1-P^-), \tag{1}$$

where Γ^l and Γ^c are the electron loss and capture rates, respectively, and $\frac{1}{2}$ is the spin-statistical factor. Loss and capture rates are influenced by the hydrogen motion parallel to the surface (translational factors) and can be obtained within the "shifted Fermi-sphere" model as follows:[2,4,12]

$$\begin{Bmatrix}\Gamma^c(Z)\\ \Gamma^l(Z)\end{Bmatrix} = \Gamma(Z)\int_0^{2\pi} d\chi \int_0^{\pi/2} |\sigma(\theta,Z)|^2 \times \sin\theta \, d\theta \begin{Bmatrix} f(\mathbf{v}_\parallel+\mathbf{k}) \\ 1-f(\mathbf{v}_\parallel+\mathbf{k})\end{Bmatrix}, \tag{2}$$

where θ and χ are the polar coordinates of the metal-state wave vector $\mathbf{k}$ with respect to the surface normal pointing towards the metal and going through the center of the atom. Z is the atom-surface distance. $\Gamma(Z)=\Gamma^c(Z)+\Gamma^l(Z)$ is the total transition rate. $|\sigma(\theta,Z)|^2$ describes the angular distribution for the electron transfer probability between the atom and the metal.[12] It is normalized using

$$2\pi\int_0^{\pi/2} |\sigma(\theta,Z)|^2 \sin\theta \, d\theta = 1. \tag{3}$$

This angular distribution does not depend on χ because of the cylindrical symmetry of the problem. $f(\mathbf{v}_\parallel+\mathbf{k})$ is the "Fermi-Dirac" function for the metal electrons viewed in the rest frame of the moving atom. The modulus of the metal electron wave vector $k \equiv |\mathbf{k}|$ is fixed by the resonance condition $k=\sqrt{2[U_0-E_a(Z)]}$. For further discussion it is useful to rearrange Eq. (1) into the form

$$\frac{dP}{dt} = (\Gamma^l + 0.5\Gamma^c)(N_{\mathrm{eq}} - P^-). \tag{4}$$

Equation (4) describes the relaxation of the negative-ion population towards the equilibrium population given by

$$N_{\mathrm{eq}} = \frac{0.5\Gamma^c}{\Gamma^l + 0.5\Gamma^c}. \tag{5}$$

The CAM method[3] is used to obtain the properties of the H^- ion in front of the metal surface: $|\sigma(\theta,Z)|^2$, $E_a(Z)$, and the total width of the affinity level $\Gamma(Z)$. We should point out that the metal is described within a ''jellium'' model in our calculations.

B. Comparison with experiment

Results of calculations are compared with experiment in Fig. 4 for Ag and in Fig. 5 for Mg. The final H^- fractions are obtained by the integration of Eq. (4) on the outgoing part of the classical trajectory of the scattered particle. The calculations were performed with two different assumptions for the initial charge state of hydrogen: H or H^-. For small exit angles (small component of the collision velocity along the surface normal: $v_\perp$) both assumptions lead to the same final charge state (see Figs. 4 and 5) and thus the calculation is parameter free. For large exit angles, the two predictions differ. The difference between the two domains of exit angles can be understood in the following way. If the exit angle and hence the normal velocity $v_\perp$ is small, the particle spends a long time in the region close to the surface [the integration of Eq. (4) starts $0.5a_0$ from the image plane]. In this region, the transition rates are very high so that a dynamical equilibrium is rapidly reached. As soon as the particle moves away from the surface the transition rates decrease. At a certain moment, the electron transfer is too slow compared to the time scale given by $v_\perp$. The charge state of the outgoing particle will not change anymore and will be ''frozen'' at the value $N_{\mathrm{eq}}(Z^*)$. Z^* is the border between fast and slow charge-transfer regions. Usually it is called the ''freezing distance'',[4] and it gives an estimate of the region where the final charge state of the system is determined. When the exit angle and $v_\perp$ increase, Z^* decreases. Typically for 1 keV it changes from $2.7a_0$ to $9.3a_0$ in the present experimental range. On the other hand, when $v_\perp$ increases, the distance needed to relax from the initial to the equilibrium population increases. Above a certain $v_\perp$, the dynamical equilibrium can no longer be reached before Z^* and the results corresponding to the two different initial conditions start to differ. For the two energies shown in the figures, the two sets of results split around the same value of $v_\perp$.

Formally, this result can be obtained from the analytical solution of Eq. (4). It has the form[4]

$$P^-(\infty)=P^-(Z_0)e^{-(1/v_\perp)\int_{Z_0}^{\infty}(\Gamma-0.5\Gamma^c)dZ} + \int_{Z_0}^{\infty} N_{\mathrm{eq}}(Z)F(Z;v_\perp,\Gamma,\Gamma^c)dZ. \tag{6}$$

The first term in Eq. (6) is called the ''memory'' term, it describes the survival of the initial ion population at Z_0. The second term in Eq. (6) describes the population formed due to the dynamical capture. $F(Z)$ is a distribution with a sharp maximum at Z^*, normalized according to

$$\int_{Z_0}^{\infty} F(Z;v_\perp,\Gamma,\Gamma^c)dZ=1.$$

If $v_\perp$ is small (small exit angles), the first term in Eq. (6) can be neglected compared to the dynamical population (second term). Increasing $v_\perp$ results in the increase of the ''memory'' term in Eq. (6). Above a certain $v_\perp$, the ''memory'' term can no longer be neglected compared to the ''dynamical'' population. This means that the two results, corresponding to different initial conditions, start to differ.

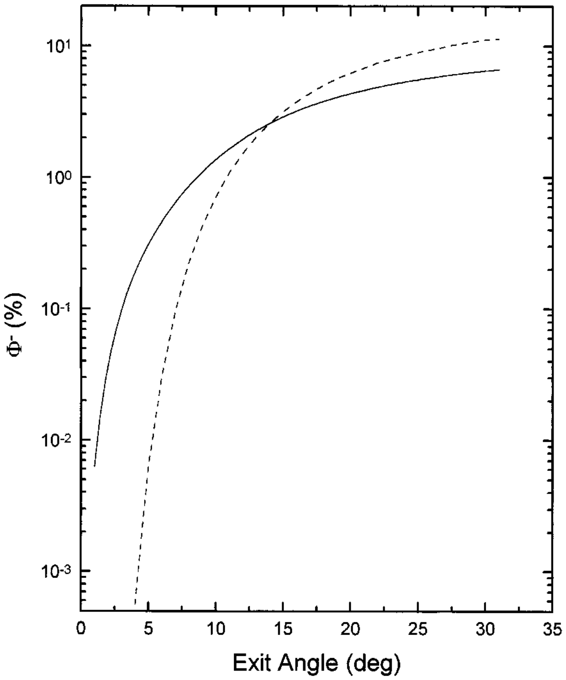

FIG. 8. Comparison of theoretical results for H^- formation on a Al target with and without the parallel velocity effect taken into account (the initial charge state of the system is neutral). Full line: with the parallel velocity effect; dashed line: without the parallel velocity effect. The incident ion energy is 2 keV.

The overall agreement between theoretical and experimental H^- fractions is rather good. For small exit angles, the experimental values are larger than the theoretical ones. This is attributed to the effect of the surface roughness as discussed above. For large exit angles, a better agreement is found for the calculations done with the system being initially a neutral H°. Close to the surface the equilibrium state of hydrogen is almost H^-, as it is inside the metal electron gas[17–19] in our velocity domain and the integration should start with the system being an ion. However, nonspecular scattering with rather large exit angles corresponds to collisions with surface atoms at small impact parameters. In such violent collisions, one can expect that any H^- ion formed in the incoming trajectory would loose its outer electron, as is observed in collisions between free atoms.[20] It is probable that even if the relaxation rates are very high close to the surface, the outgoing particle is still neutral when it arrives in the image plane region, where the integration of Eq. (4) is started. This could explain the better agreement with experiment at large angles obtained for the neutral initial condition.

It is noteworthy that, similarly to the experimental data, the present theoretical results for 1 and 4 keV almost scale when plotted as a function of $v_\perp$. However, this is not a proof of the absence of the parallel velocity effect, test calculations neglecting it leading to very different results. Figure 8 presents theoretical results for H^- formation on a Al target with and without the parallel velocity effect taken into account (the initial charge state of the system is neutral). As can be seen, the two results are different, especially for the small scattering angles, when the neglect of the $\vec{v}_\parallel$ effect leads to a very strong underestimation of the negative ion formation probability. These differences can be analyzed using the so-called ''freezing distance approximation'' (Secs. IV A, IV B and see Refs. 4 and 13) which states that the final ion fraction is equal to $N_{\mathrm{eq}}(Z)$. This approach is only an approximation to the exact results presented in Figs. 4, 5, 7, and 8; although not perfect, it can be used for a qualitative discussion of the ion fraction. If the parallel velocity effect is neglected the quantity N_{eq} given by Eq. (5) sharply switches from 1 to 0 when z increases above Z_e, the crossing distance between the H^- level and the Fermi level. When the scattering angle increases in the experimental range, the freezing distance Z^* moves from below to above Z_c. This is reflected in Fig. 8, where the H^- formation probability (no $\vec{v}_\parallel$ effect) is extremely small at small angles and large at large angles. Indeed Φ^- does not switch from 0 to 1 due to the defect of the freezing approximation. When the $\vec{v}_\parallel$ effect is taken into account, it results in a softening of the transition between 1 and 0 for $N_{\mathrm{eq}}(Z^*)$. At large distances, due to the shift of the Fermi sphere, electron capture becomes possible and N_{eq} goes from zero to a finite value; this leads to a strong relative increase of the final ion fraction at small angles. In contrast, at small distances, the Fermi sphere shift results in the existence of an electron-loss channel, i.e., N_{eq} decreases from 1 to a finite value; this leads to a decrease of the final ion fraction at large angles. This relative decrease is less important than the relative increase found at small angle which corresponds to an increase from a vanishingly small value. This then accounts for the very strong effect of the parallel velocity at small angles and the rather moderate opposite one at large angles.

C. Influence of the band characteristics and of the angular distributions on the charge transfer

In Fig. 7, we present the theoretical results for 2-keV hydrogen scattering on Mg, Al, and Ag surfaces (neutral initial condition). These compare well with the corresponding experimental results of Fig. 7. In particular, the relative magnitude of the ion fractions for the three targets is well reproduced. As mentioned above, in these three systems with rarther high work functions, the parallel velocity effect plays a critical role in negative-ion formation. It allows the matching of the energy level of the anion and those of the occupied metal states. A discussion of the relative value of the three ion fractions should then include a discussion of the relative efficiency of the parallel velocity effect in these three systems and should not be limited to a comparison of the work functions. As discussed above this is particularly important at small scattering angles. At large scattering angles the $\vec{v}_\parallel$ effect is less important and the work function may be expected to be a very effective parameter.

The difference between the three results can be analyzed using the ''freezing distance'' approximation. As we have shown in a previous study,[21] the energy and the lifetime of an H^--ion interacting at large distances with a jellium metal surface are not very dependent on the characteristics of the jellium. As a consequence, the freezing distance Z^* is roughly the same for the three systems. In addition, since the capture rate is much smaller than the total rate (ion fractions are very small), N_{eq} given by Eq. (5) is roughly equal to half the ratio between the capture and total rate, i.e., to half the value of the integral over θ and χ:

$$N_{\mathrm{eq}}=\frac{1}{2}\int_0^{2\pi}d\chi\int_0^{\pi/2}|\sigma(\theta,Z)|^2\sin\theta\,d\theta\,f(\mathbf{v}_\parallel+\mathbf{k}). \quad (7)$$

If one further assumes a 0 K temperature of the surface, then the above integral reduces to the integral of $|\sigma(\theta,Z)|^2$ over the k directions that are inside the Fermi sphere (see Fig. 1). The equilibrium population (7) indeed depends on the relative position of the ion level and the Fermi level. In the absence of the parallel velocity effect this is the only parameter and $N_{\mathrm{eq}}(Z^*)$ is equal to zero or 1. However, in the present cases, where a strong parallel velocity effect is present, $N_{\mathrm{eq}}(Z^*)$, given by Eq. (7), is much influenced by it. It is given by the weighted overlap between two spheres [Eq. (7)] and so, depends on the relative sphere radii. These are given by a few parameters: the ion level, the Fermi energy, and the surface work function. The influence of these parameters is further illustrated below.

A first estimate can be made with an isotropic $|\sigma(\theta,Z)|^2=1/2\pi$. In this case, as follows from Eq. (2), the equilibrium population, i.e., the ion fraction is proportional to the fraction of the electronic states in $\mathbf{k}$ space having energy U_0-E_a and which are in resonance with occupied states of the metal. This is purely a geometrical factor given by the overlap between the k sphere and the Fermi sphere shifted by $\mathbf{v}_\parallel$ in Fig. 1. In Fig. 9(a) we present this geometrical factor as function of the parallel velocity for an atom-surface distance of $7a_0$, which represents a typical ''freezing'' distance. It is seen that the largest equilibrium population is obtained for the Al target. Consequently, one would expect the largest H^- fraction for this system. So, the geometrical factor alone is not able to predict the relative value of the ion fractions and furthermore it is not linked with the relative value of the surface work functions.

The situation changes dramatically when the angular distribution is introduced into the calculation. Results, presented in Fig. 9(b) reveal an equilibrium population (and correspondingly a negative-ion fraction) for Mg that is three times larger than that for Al and Ag. The last two are comparable. This result gives a relative order of magnitude for the three targets that is consistent with the experimental observations and the predictions of the exact solution of Eq. (4). (Our experimental results correspond to parallel velocity values in the range of 0.2–0.4 a.u.) This result is directly related to the shape of the angular distributions $|\sigma(\theta,Z)|^2$ for an H^--surface distance of $7a_0$, which are shown in Fig. 9 (in the figure, the distributions have been normalized to 1 at the maximum for the sake of comparison). These are rather narrow and point in the direction of the surface normal. As can be seen, the angular distribution for Al is much narrower than that for Ag and Mg. This can be linked with the properties of the metal bands and is totally independent of the surface work function. Indeed, the transition rate between the negative-ion state and a given metal state $|\mathbf{k}\rangle$ is larger for metal states having a larger wave-function extension into the vacuum. The vacuum tail of the metal electron states which

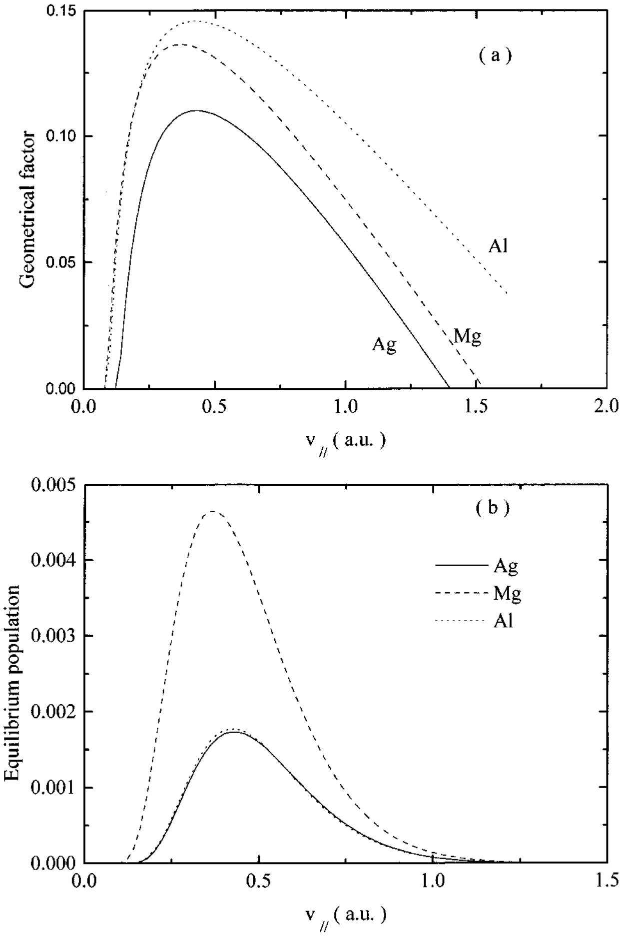

FIG. 9. (a) Geometrical factor given by the overlap between the k sphere and the Fermi sphere shifted by $\mathbf{v}_{\parallel}$. The parallel velocity is given in atomic units (1 a.u.$=2.19\times10^6$ m/s). (b) Equilibrium population when the angular distributions are taken into account.

are in resonance with the negative-ion level is determined by E_b the electron binding energy in the direction of the surface normal.

$$E_b = U_0 - (U_0 - E_a)\cos^2\theta = U_0 \sin^2\theta + E_a \cos^2\theta. \tag{8}$$

From Eq. (6) we conclude that the larger U_0 is, the faster E_b increases when θ increases. This leads to a faster decrease of the vacuum tail of the metal electron wave function. Consequently, the larger U_0 is the narrower the angular distribution is. This is exactly what can be seen in Fig. 10. Since the integration in Eq. (7) is performed in the wings of the angular distribution, it is very sensitive to the width of the angular distribution and this accounts for the large modifications introduced in the equilibrium fractions.

Finally, one can conclude that the differences between the different ion fractions for the different targets are directly related to the characteristics of the valence bands. The relative values of the ion fractions are due to the interplay of a geometrical factor determined by the energetics of the problem including the surface work function and of the angular dependence of the transition probabilities.

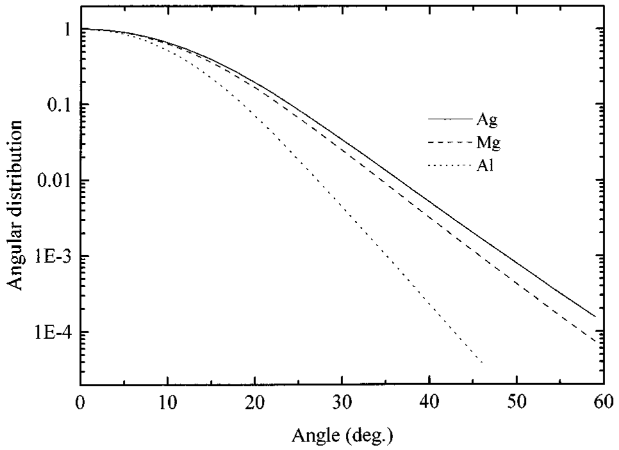

FIG. 10. Angular distributions calculated for various metals. The polar angle (θ) for the electron ejection into the metal is measured with respect to the surface normal.

D. Comments on positive-ion fractions

We shall not discuss the small positive-ion fractions in detail here. In the case of Mg it does not depend on the exit angle. As mentioned above this fraction is the same independently of the charge state of the incident ion. We must therefore envisage ionization processes following neutralization of incoming ions. It is known from studies of gas phase collisions of hydrogen atoms with Mg vapor targets that H^+ ions are produced.[22] The cross section is quite small in the low keV energy range. It increases rapidly by an order of magnitude with increasing energy in the 1–10-keV range. One could also expect the existence of ionization in binary collisions here. Furthermore, ionization may occur via a kinematic Auger loss mechanism (Fig. 1).[23] As may be deduced from this figure, the energy-conservation requirement for this process is

$$\frac{(v_F+v_i)^2}{2} - (v_F - v_i)^2 = E_a - \epsilon_F - \phi, \tag{9}$$

where v_F and v_i are Fermi and ion velocities and E_{at} the ionization potential of the atom. Assuming a $4a_0$ atom surface distance, which would lead to a 1.7-eV shift of the H energy level, we find that the threshold velocity requirement for Mg is of $v_i = 0.14$ a.u. This velocity corresponds to a hydrogen atom with a 490-eV energy. For Ag this would occur for a velocity of 0.15 a.u. corresponding to a 560 eV. Thus H^+ production we observe may be due to both collisional and the dynamic Auger ionization processes. At present it does not appear possible to estimate the proportion of H^+ formed at small distances and which should eventually be taken into account in the calculation of negative-ion formation.

V. CONCLUSIONS

We present the results of an experimental and theoretical investigation of H^- formation in collisions of 1 to 4-keV positive and negative hydrogen ions with clean Mg, Al, and

Ag surfaces. The scattered ion fractions were measured in a large angular range extending from 2° to 40° with respect to the surface plane. This allowed us to study the characteristics of the resonant charge-transfer process for conditions of fairly high velocities normal to the surface, when small atom surface distances play an important role. The theoretical analysis we presented revealed the role played by the metal bandwidth in this dynamical capture process.

Note added in proof. A theory of H^+ production in swift hydrogen atom scattering has been recently developed by Flores and co-workers.[24]

ACKNOWLEDGMENTS

The authors would like to thank T. Schlatholter and S. Ustaze for help in the final stages of the experiments.

---

[1] M. Maazouz, R. Baragiola, A. Borisov, D. Teillet-Billy, V. A. Esaulov, S. Lacombe, J. P. Gauyacq, and L. Guillemot, Surf. Sci. **364**, L568 (1996).

[2] J. N. M. van Wunnick, R. Brako, K. Makoshi, and D. M. Newns, Surf. Sci. **126**, 618 (1983).

[3] R. Brako and D. M. Newns, Rep. Prog. Phys. **52**, 655 (1989).

[4] J. Los and J. J. C. Geerlings, Phys. Rep. **190**, 133 (1990).

[5] R. Zimny, H. Nienhaus, and H. Winter, Radiat. Eff. Defects Solids **109**, 9 (1989).

[6] D. Teillet-Billy and J. P. Gauyacq, Surf. Sci. **229**, 343 (1990).

[7] F. Wyputta, R. Zimny, and H. Winter, Nucl. Instrum. Methods Phys. Res. Sect. B **58**, 379 (1991).

[8] V. Esaulov, L. Guillemot, O. Grizzi, M. Huels, S. Lacombe, and Vu Ngoc Tuan, Rev. Sci. Instrum. **67**, 1 (1996).

[9] V. Esaulov, D. Dhuicq, and J. P. Gauyacq, J. Phys. B **11**, 1049 (1978).

[10] S. Haussman, C. Höfner, T. Schlatholter, H. Franke, A. Närman, and W. Heiland, Nucl. Instrum. Methods Phys. Res. Sect. B **115**, 31 (1996).

[11] M. Shi, J. W. Rabalais, and V. Esaulov, Radiat. Eff. Defects Solids **109**, 81 (1989).

[12] A. Borisov, D. Teillet-Billy, and J. P. Gauyacq, Surf. Sci. **278**, 99 (1992).

[13] E. G. Overbosch and J. Los, Surf. Sci. **108**, 99 (1981).

[14] J. J. C. Geerlings, J. Los, J. P. Gauyacq, and J. N. M. Temme, Surf. Sci. **172**, 257 (1986).

[15] R. Zimny, Surf. Sci. **233**, 333 (1990).

[16] D. C. Langreth and P. Nordlander, Phys. Rev. B **43**, 2541 (1991).

[17] P. M. Echenique, F. Flores, and R. H. Ritchie, Solid State Phys. **43**, 229 (1990).

[18] P. M. Echenique and F. Flores, Phys. Rev. B **35**, 8249 (1987).

[19] M. Penalba, A. Arman, P. M. Echenique, F. Flores, and P. M. Ritchie, Europhys. Lett. **19**, 45 (1992).

[20] V. Esaulov, Ann. Phys. (Paris) **11**, 493 (1986).

[21] D. Teillet-Billy and J. P. Gauyacq, Surf. Sci. **269/270**, 162 (1992).

[22] K. H. Berkner, R. V. Pyle, and J. W. Stearns, Phys. Rev. **178**, 248 (1969).

[23] R. Zimny and Z. L. Miskovic, Nucl. Instrum. Methods Phys. Res. Sect. B **58**, 387 (1991).

[24] J. Merino, N. Lorente, F. Flores, and M. Yu. Gusev, Nucl. Instrum. Methods Phys. Res. (to be published).